Supporting Information for

Synergistic enhancement of the electrocatalytic reduction of CO_2 to hydrocarbons at large-sized Cu@Ag electrode

Ke-Ke Chang[ab], Wan-Feng Xiong[b], Yu-Ting Wen[b], Bin-Bin Feng[ab], Hong-Fang Li*[bde], Teng Zhang[bde], Yuan-Biao Huang[be], Duan-Hui Si*[bde] and Rong Cao*[bcde]

[a]*College of Chemistry and Materials Science, Fujian Normal University, Fuzhou 350007, China*

[b]*State Key Laboratory of Structural Chemistry, Fujian Institute of Research on the Structure of Matter, Chinese Academy of Sciences, Fuzhou 350002, China*

[c]*Fujian College, University of the Chinese Academy of Sciences, Fuzhou, Fujian 350002, China*

[d]*Fujian Science & Technology Innovation Laboratory for Optoelectronic Information of China, Fuzhou , Fujian, 350108, P. R. China*

[e]*University of Chinese Academy of Sciences, Beijing 100049, China*

E-mail: rcao@fjirsm.ac.cn; siduanhui@fjirsm.ac.cn; hongfangli@fjirsm.ac.cn

Materials and Synthetic Procedures

All reagents and chemicals were acquired from commercial sources and used. All aqueous solutions were prepared with Ultrapure water (18.25 MΩ·cm).

Synthesis of pristine Ag foil: The silver foil (0.1 mm thickness, 99.999%, Alfa Aesar) was subjected to an acid wash and sonication for 30 minutes using 0.1 M HCl, followed by a rinse with deionised water and storage under nitrogen.

Synthesis of Cu@Ag catalyst: The electrodeposition of Cu@Ag catalyst was conducted in a three-electrode electrochemical cell utilising polished (0.1 M HCl) silver foil (0.1 mm thickness, 99.999%, Alfa Aesar) as the working electrode, Pt (99.99+%, Goodfellow) as the counter electrode and Ag/AgCl (Biologic) as the reference electrode. A mixed solution of 0.1 M $KHCO_3$ and 0.1 M KCl was added with 0.2 M $CuSO_4$ as the electrolyte, and electrodeposition was carried out by CV scanning method with scanning potentials of 0 – -1.5 V vs. RHE, with a total of 40 scanning turns. Subsequently, the catalysts were removed from the electrolytic bath, rinsed with Milli-Q water, and then dried and preserved with N_2 gas.

Synthesis of bare Cu naoparticle: Electrodeposition of bare Cu NPs was carried out in a three-electrode electrochemical cell using carbon paper as the working electrode, Pt (99.99+%, Goodfellow) as the counter electrode and Ag/AgCl (Biologic) as the reference electrode. A mixed solution of 0.1 M $KHCO_3$+0.1 M KCl was added with 0.2 M $CuSO_4$ as electrolyte and electrodeposition was carried out by CV scanning method with scanning potentials of 0 – -1.5 V vs. RHE and scanning circle number of 40. Immediately after deposition, the catalysts were taken out from the electrolytic bath, rinsed with milliq water, and then blown dry and preserved with N_2 gas.

Silver-plated copper: Purchase from Hetianxia Metals, and its structure was characterized by SEM and XRD. The thickness of the outer Ag was 500 nm.

Methods

Characterization

Powder X-ray diffraction (PXRD) patterns were recorded on a Miniflex-600 diffractometer using Cu Kα radiation (λ = 0.154 nm). X-ray photoelectron spectroscopy (XPS)

measurements were performed on an ESCALAB 250Xi X-ray photoelectron spectrometer (Thermo Fisher) using an Al Ka source (15 kV, 10 mA). (the C-C peak here were corrected to 284.8 eV). Operando attenuated toal reflectance Fourier transform infrared spectroscopy (ATR-FTIR) was obtained by a Nicolet 6700 (Thermo Fisher) equipped a liquid nitrogen cooled MCT detector. Experiments were performed at the potential of -1.4 V in the mixture of 0.1 M $KHCO_3$ and 0.1 M KCl using a home-made ATR-FTIR setup. Electrochemical CO_2 reduction reaction atalyst was used as the working electrode, with the Ag/AgCl electrode as the reference electrode and Pt wire as the counter electrode. The gas inlet and outlet used to purge Ar/CO_2 were present on the cell wall. The working electrode must touch the Ge crystal surface, so that the IR beam can probe the intermediate species formed during CO_2 reduction. The electrochemical cell was first purged with Ar for 30 min. CO_2 was then purged into the cell at a flow rate of about 30 mL min^{-1} for another 30 min. After that, a background IR spectrum was taken. A fixed potential -1.5 V vs. RHE was then applied to the working electrode. In the meanwhile, with CO_2 continuously purging, real-time spectra were collected at a resolution of 4 cm^{-1} and 32 interferograms were co-added for each spectrum with a collection period of 50 s.

Electrochemical measurements

In the airtight three electrode H electrolytic cell separated by proton-exchange membrane, the platinum mesh and Ag/AgCl are the counter electrode and the reference electrode respectively. 35 ml of 0.1 mol/L $KHCO_3$ + 0.1 mol/L KCl mixed electrolyte is filled in the electrolytic cell, the working electrode and the reference electrode are placed in the cathode cell, the counter electrode is placed in the anode cell, the device is sealed, and the high-purity carbon dioxide gas is continuously injected into the cathode cell at a ventilation rate of 30 ml per minute. Before the CO_2 electrochemical reduction, the electrolyte in the cathodic compartment was purged with CO_2 gas for at least 30 min to achieve the CO_2-saturated solution (pH = 6.8) When the gas reaches saturation, conduct cyclic voltammetric scanning. The scanning speed is 100 mV · s^{-1}, and the scanning range is 0 to -0.9 V vs. RHE (all indicated potentials have been converted to the potential of the standard hydrogen electrode). The number of scanning cycles is 10. The role of this step is to clean the catalyst surface and

play a certain role in activation. The performance test of electrocatalytic carbon dioxide was conducted using a linear voltammetry curve to characterize the catalyst activity, with a scanning speed of 10 mV · s^{-1} and a scanning range of 0 to -1.6 V vs. RHE. In the studies, all potentials were converted to potential vs. reversible hydrogen electrode (RHE) according to the equation E (vs RHE) = E (vs Ag/AgCl) + 0.196 V + 0.059 × pH, without IR compensation. CO_2 gas was delivered at an average rate of 30 mL min^{-1}(at room temperature and ambient pressure) and routed into the gas sampling loop (1mL) of a gas chromatograph. The gas phase composition was analyzed by gas chromatograph (GC) equipped with flame ionization detector (FID). Selective testing of electrocatalytic carbon dioxide reduction: Using chronoamperometry, the gas products generated were collected from -0.9V vs. RHE to -2.0 V vs. RHE for 30 minutes at each potential.

The Faraday efficiency of a certain gas product was calculated based on the following equations:

$$FE = \frac{PV}{T} \times \frac{vNF \times 10^{-6}(m^3 / mL)}{I \times 60(\mathrm{s} / \mathrm{min})}$$

v (vol %): volume concentration of certain gas product in the exhaust gas from the cell (GC data);

V: gas flow rate measured by a flow meter, 30 mL min^{-1};

I: total steady-state cell current;

N: the electron transfer number for product formation;

F: Faradaic constant, 96485 C mol^{-1};

R: universal gas constant, 8.314 J mol^{-1} K^{-1};

P: one atmosphere, 1.013 105Pa;

T: room temperature, 298.15 K.

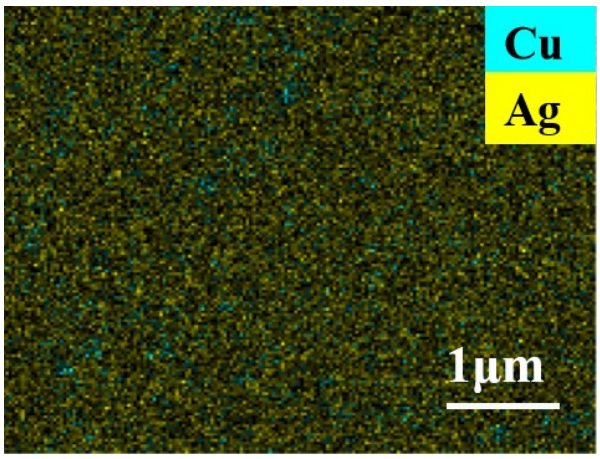

Figure S1. Mapping image of Cu@Ag catalyst.

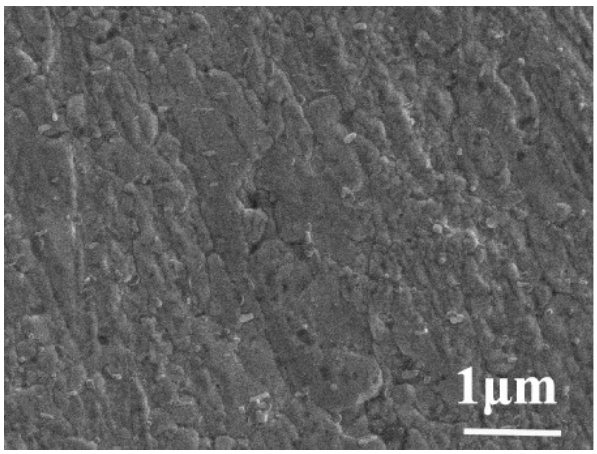

Figure S2. SEM image of pristine Ag foil.

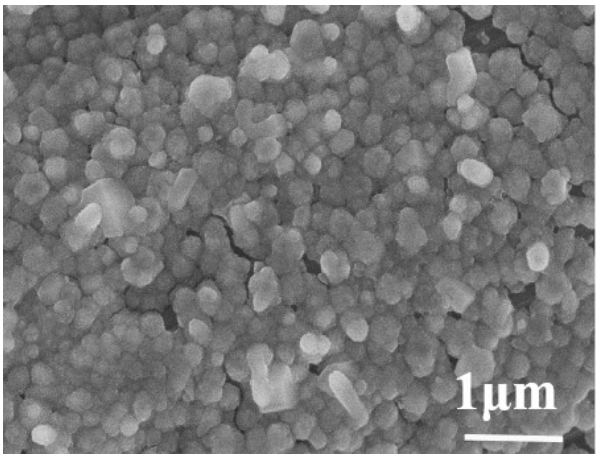

Figure S3. SEM image of bare Cu NPs prepared by electrodeposition on carbon paper surface.

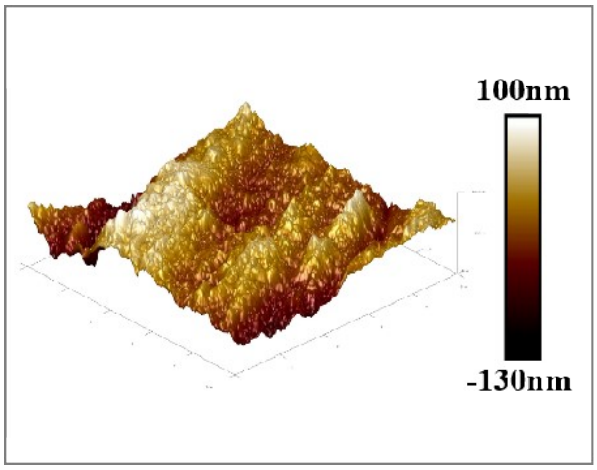

Figure S4. AFM image of pristine Ag foil with low roughness of 22.1 nm.

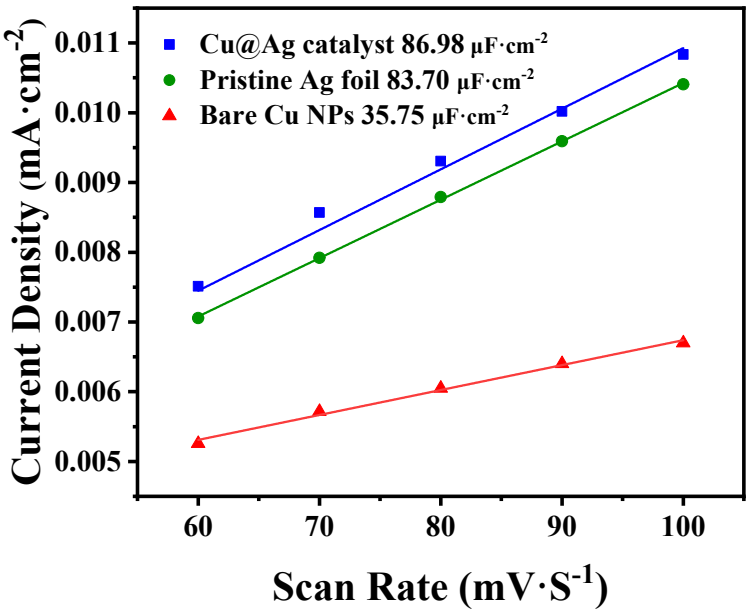

Figure S5. Electrochemical active surface areas of Cu@Ag catalyst, bare Cu NPs and pristine Ag foil.

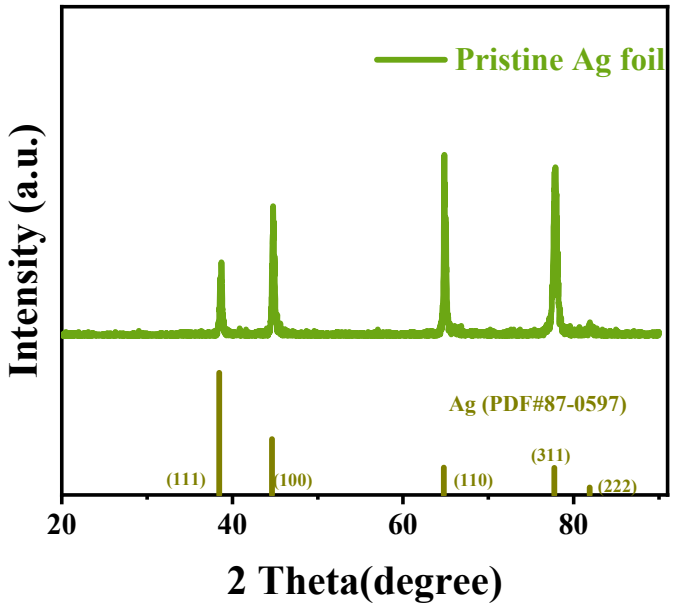

Figure S6. XRD image of acid-washed pristine Ag foil, with the green line representing the reference samples with PDF numbers 87-0597.

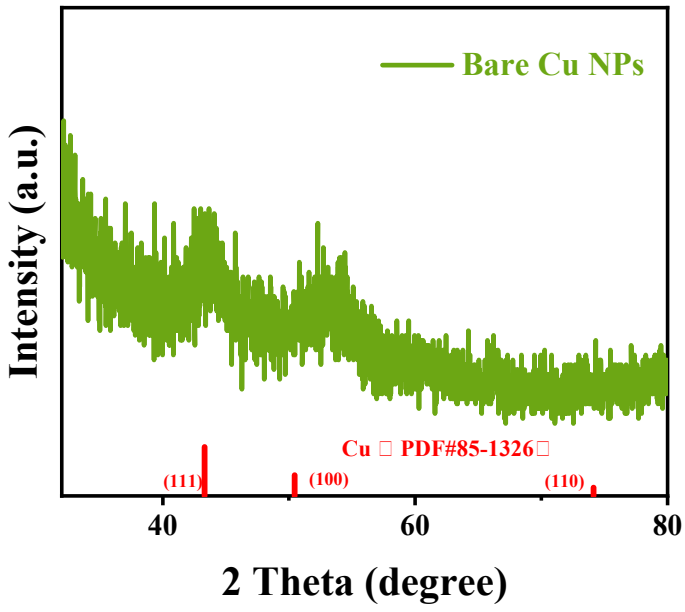

Figure S7. XRD image of bare Cu NPs prepared by electrodeposition on carbon paper, with the red line representing the reference samples with PDF numbers 85-1326.

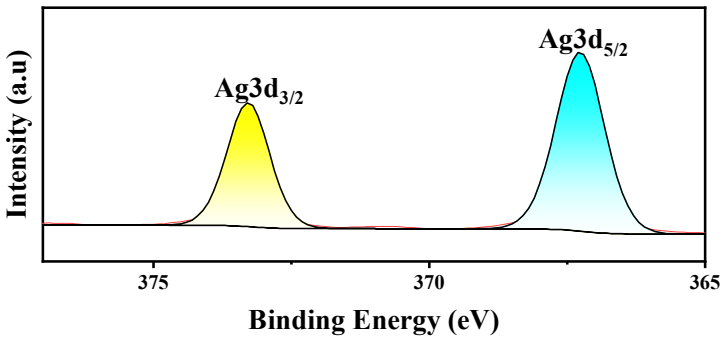

Figure S8. XPS spectra of Ag 3d of pristine Ag foil.

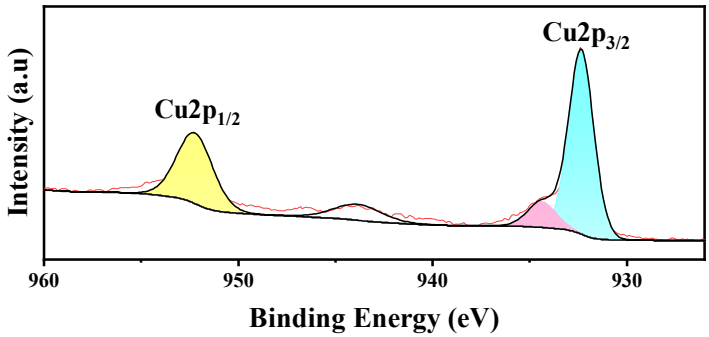

Figure S9. XPS spectra of Cu 2p of bare Cu NPs prepared by electrodeposition on carbon paper surface.

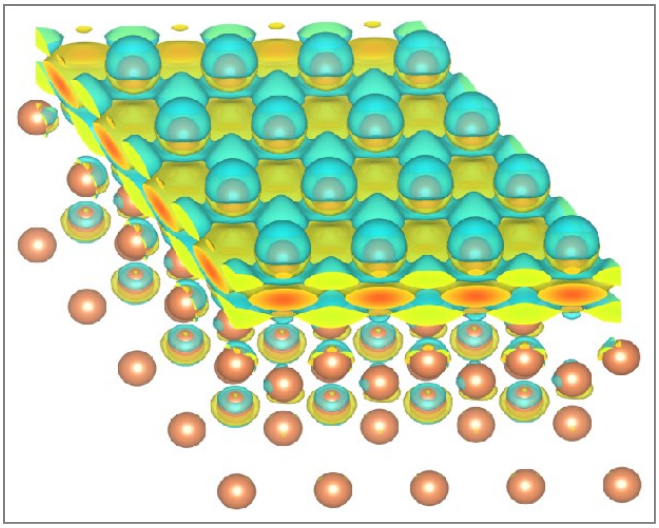

Figure S10. Charge density difference of bare Cu NPs (the cyan region reflects an electron-deficient state, whereas the yellow region reflects an electron-rich area).

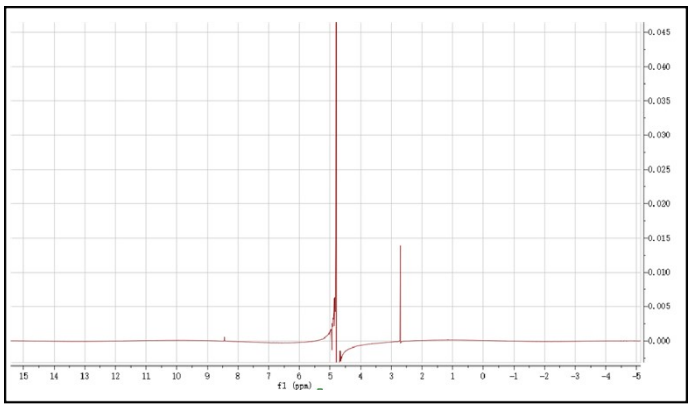

Figure S11. 1H Nuclear Magnetic Resonance (NMR) Spectroscopy of Liquid Phase Products.

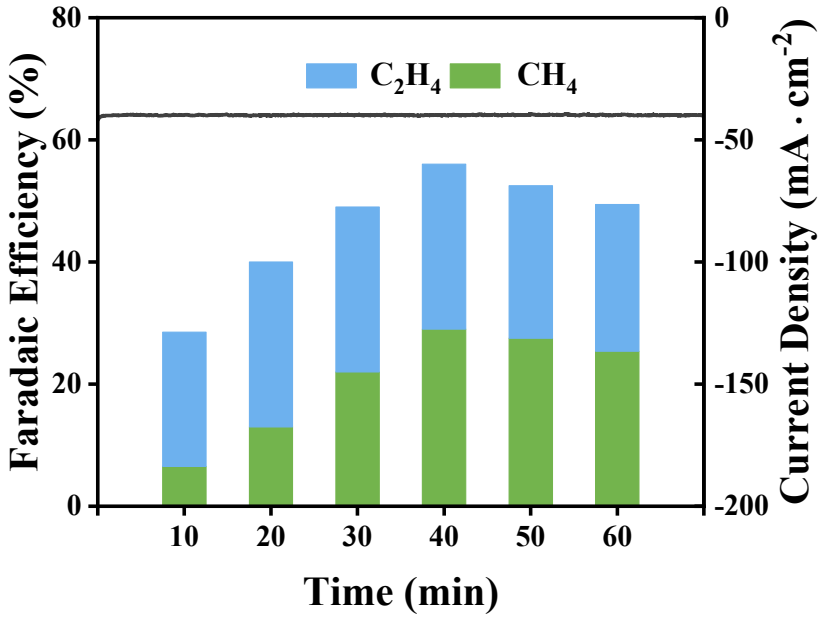

Figure S12. The current density and FE of CH_4 and C_2H_4 over 60 minutes electrolysis as a function of applied potential on Cu@Ag catalyst.

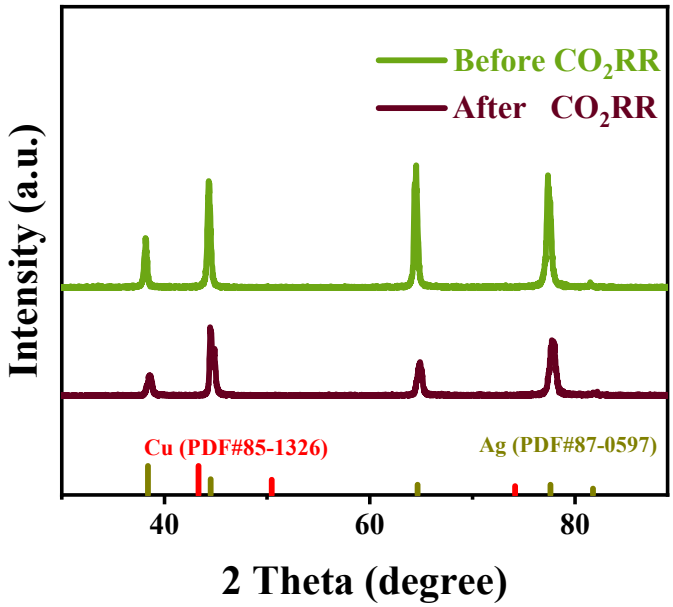

Figure S13. The XRD of Cu@Ag catalyst after CO_2RR, with the green line representing the reference samples with PDF numbers 87-0597 and the red line representing the reference samples with PDF numbers 85-1326.

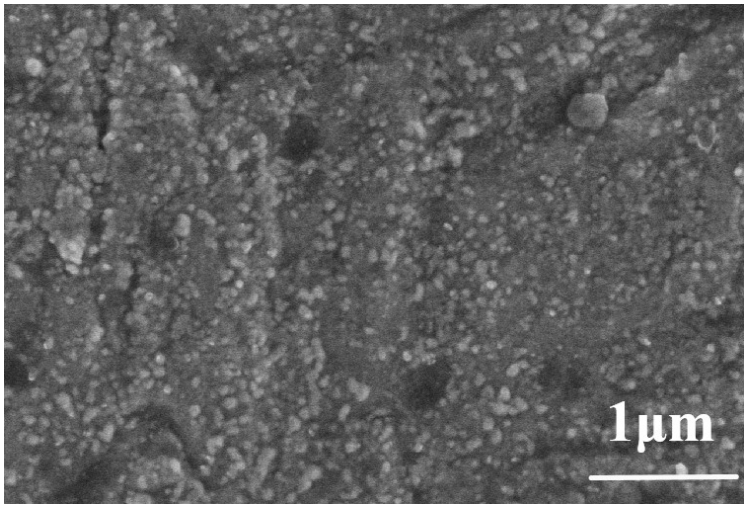

Figure S14. SEM image of Cu@Ag catalyst after CO_2RR.

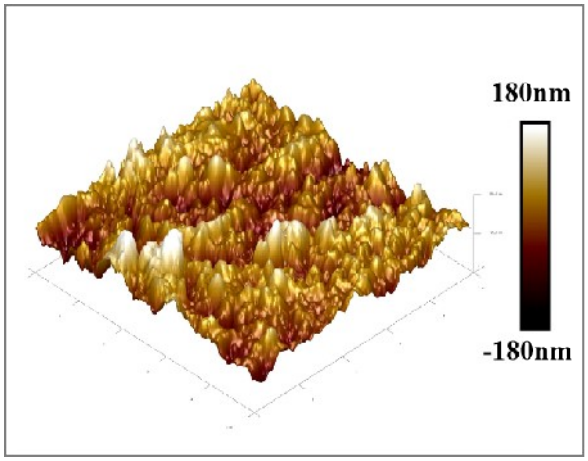

Figure S15. AFM image of Cu@Ag catalyst after CO_2RR.

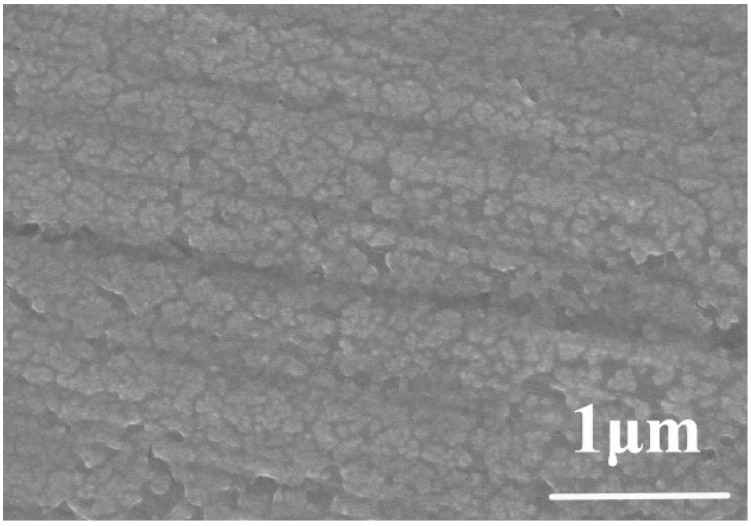

Figure S16. SEM image of bare Cu NPs after CO_2RR.

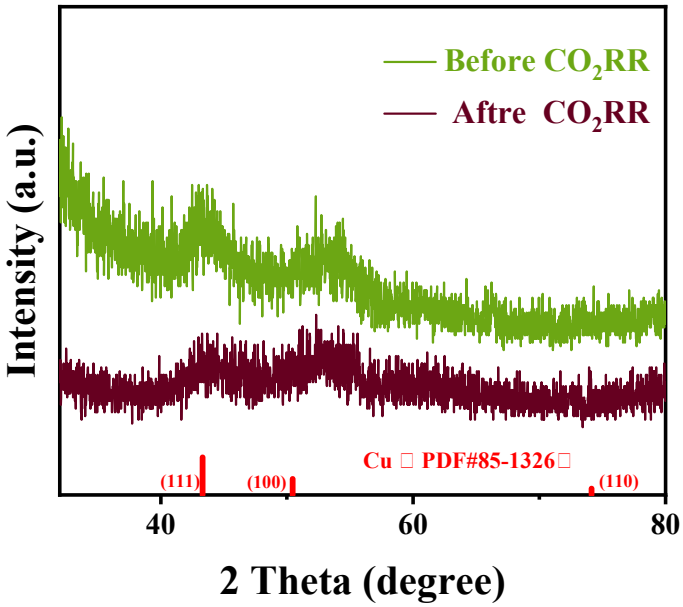

Figure S17. The XRD of bare Cu NPs after CO_2RR, with the red line representing the reference samples with PDF numbers 85-1326.

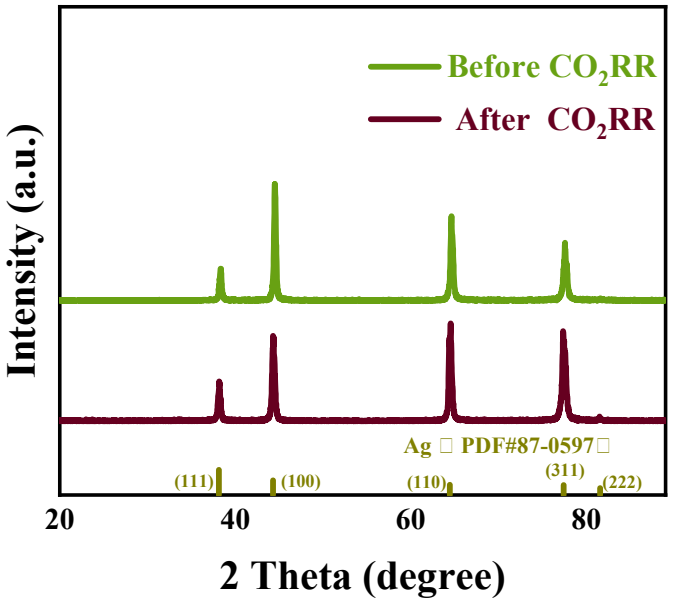

Figure S18. The XRD of pristine Ag foil after CO_2RR, with the green line representing the reference samples with PDF numbers 87-0597.

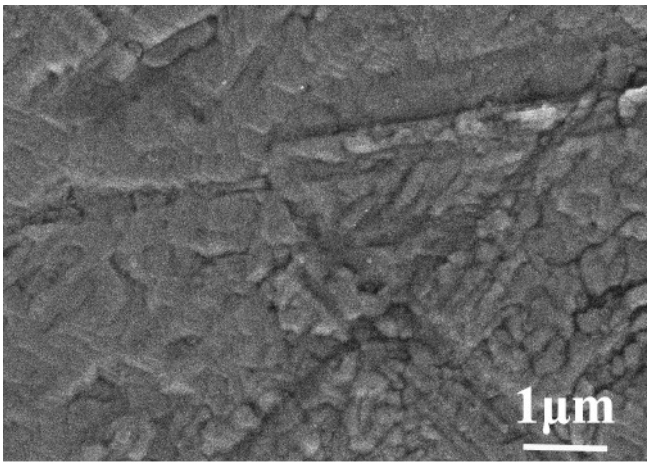

Figure S19. SEM image of pristine Ag foil after CO_2RR.

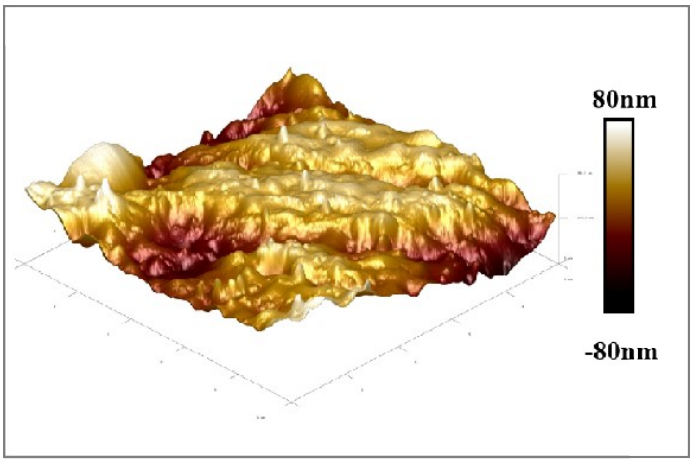

Figure S20. AFM image of pristine Ag foil after CO_2RR.

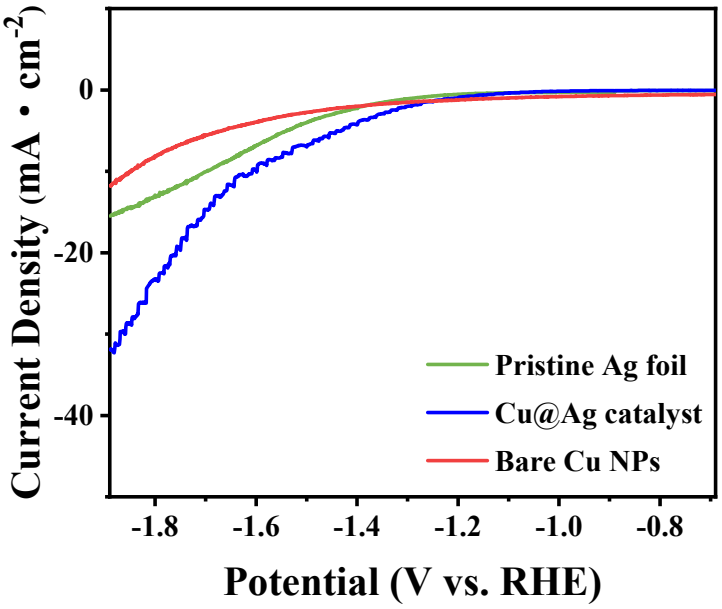

Figure S21. The LSV of Cu@Ag catalyst, bare Cu NPs and pristine Ag foil in CO_2 atmosphere.

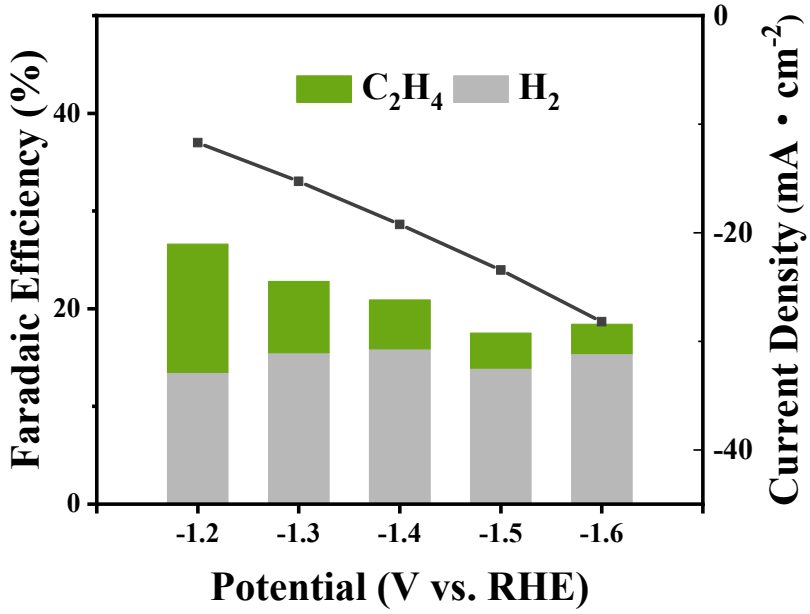

Figure S22. Faradaic efficiency for CORR over bare Cu NPs at different potentials.

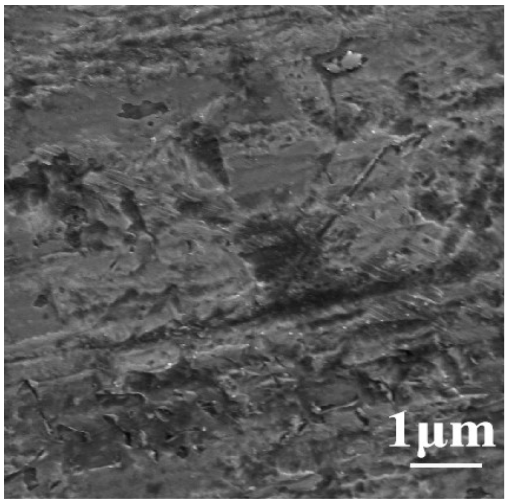

Figure S23. SEM image of Ag-plated Cu.

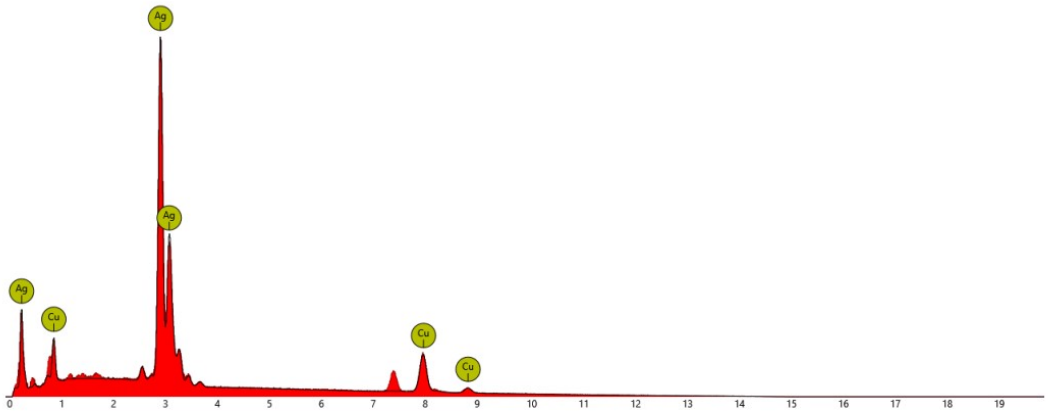

Figure S24. Elemental composition of Ag-plated Cu

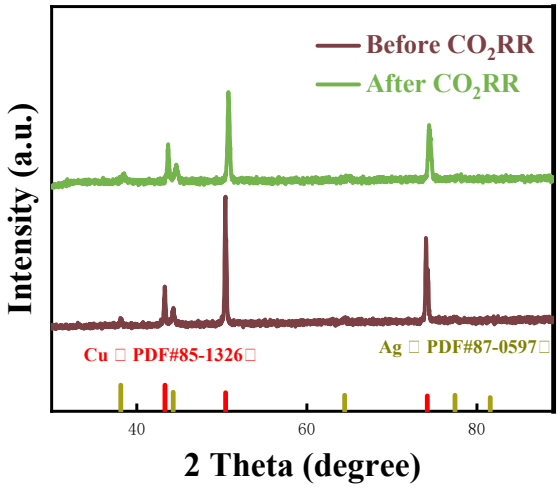

Figure S25. The XRD of Ag-plated Cu after CO_2RR, with the green line representing the reference samples with PDF numbers 87-0597 and the red line representing the reference samples with PDF numbers 85-1326.

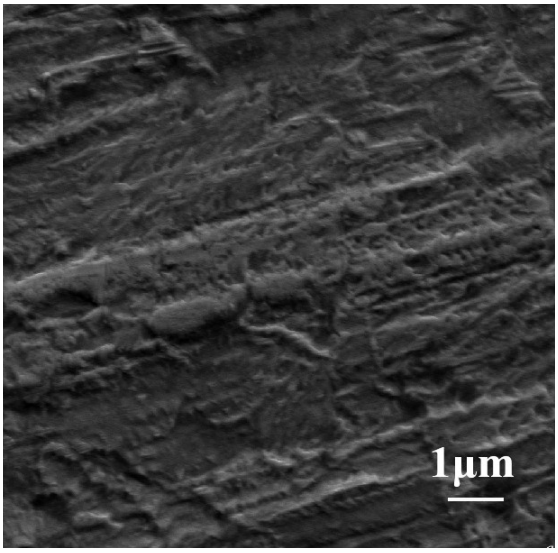

Figure S26. SEM image of Ag-plated Cu after CO_2RR.

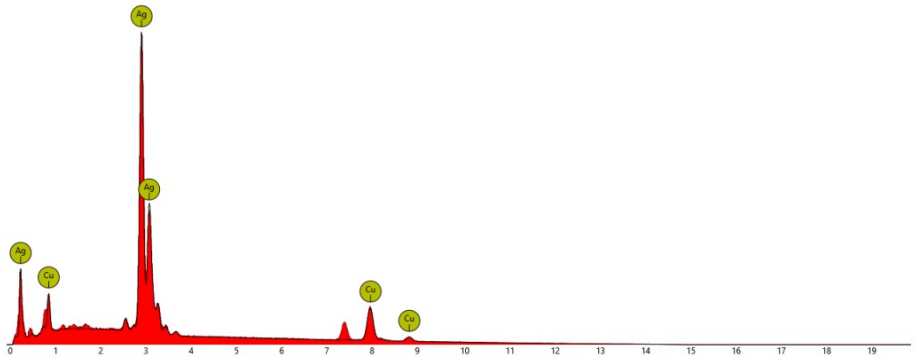

Figure S27. Elemental composition of Ag-plated Cu after CO_2RR.

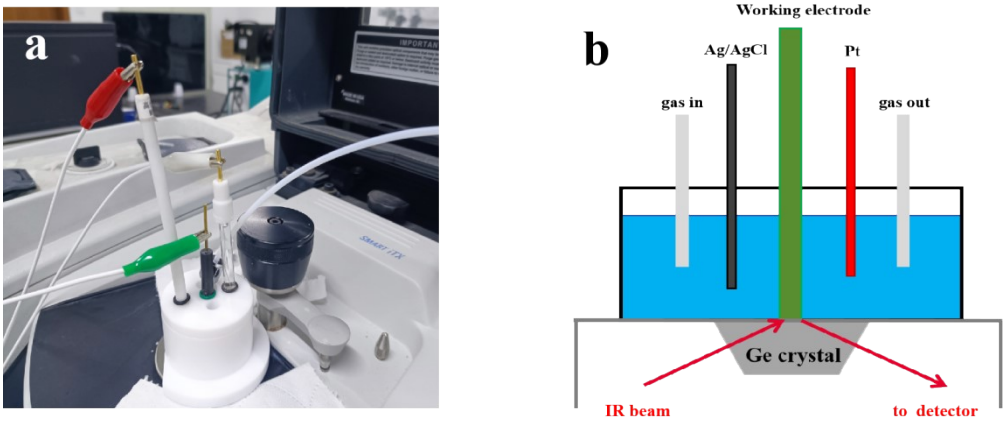

Figure S28. The home-made cell used for operando ATR-FTIR measurements (a) Cell in use and (b) Schematic illustration of the home-made cell.

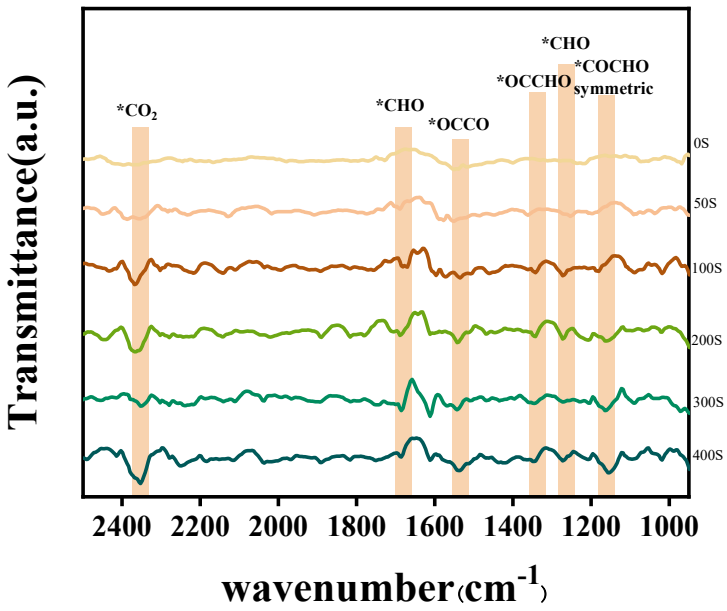

Figure S29. *In situ* ATR-FTIR spectra of Cu@Ag catalyst at different time. The measurements were obtained in an electrolyte solution containing 0.1 M $KHCO_3$ and 0.1 M KCl at the potential of -1.5 V vs. RHE.

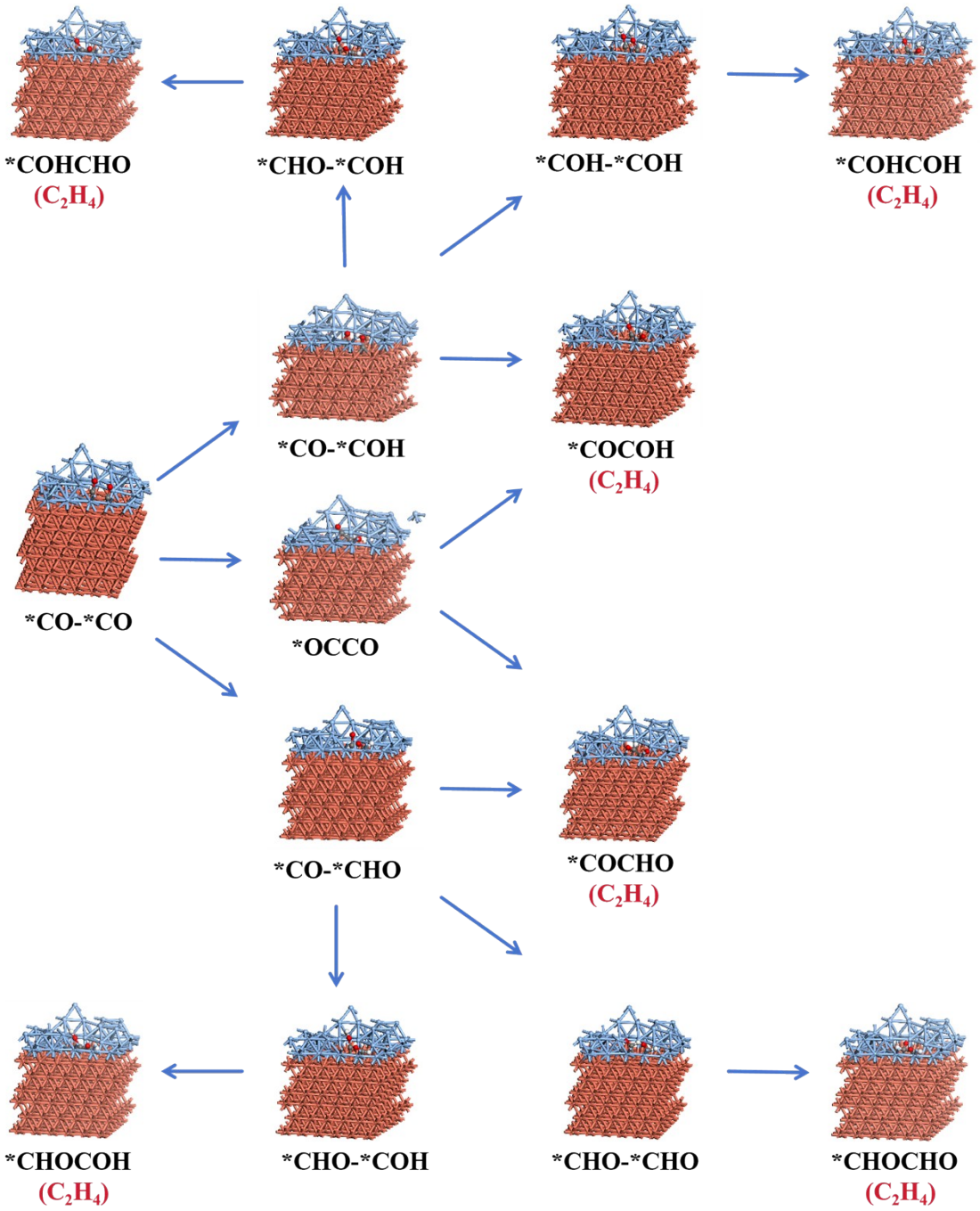

Figure S30. The multiple CO_2RR pathway toward C_2H_4 product on Cu@Ag catalyst, Ag(light blue), Cu (orange), O (red), H (white), C (dark grey).

Table S1. Summary of CO_2RR to hydrocarbons on Cu-Ag bimetallic catalysts in a H-cell.

Catalyst	E (vs. RHE)	CH_4 FE(%)	C_2H_4 FE(%)	Reference
Cu@Agcatalyst	-1.5 V	26.8	33	This work
Cu-Ag NC	-1.2V	14.2	30.7	1
Cu_{cub}-Ag	-1.3V	5.2	16.8	2
Ag-Cu dual cathode	-1.4V	4.6	8.0	3
$Cu_{8.2}Ag_{1.8}$NWs	-0.6V	33.8	11.2	4
Cu/Ag(s)	-1.2V	＜5.0	＜5.0	5
Cu-Ag@NC	-1.0V	＜5.0	＜15.0	6
Ag@Cu-20	-1.06V	＜20.0	28.6	7
$Ag_{91}Cu_9$	-1.0V	＜5.0	＜1.0	8
$Cu_{50}Ag_{50}$	-0.9V	＜5.0	＜10.0	9

Computational methods

To confirm the speculation of the Cu-Ag interface has a higher electron density favourable for stabilising *CHO intermediates, facilitating the coupling of *CHO and *CO intermediates to form C_2H_4, the mechanism of CO_2RR on the *CHO and *CO intermediates at the Cu-Ag interface and on the Cu surface were calculated by density functional theory (DFT) calculations through Vienna Ab initio Simulation Package (VASP)[10-12] .Pseudopotentials were conducted by the Perdew-Burke-Ernzerh (PBE) exchange-correlation functional[13] and the projector-augmented wave (PAW)[14] In the intermediates optimizations, the convergence criteria and the cutoff energy of plane wave basis were set to 1×10^{-4} eV and 400 eV, respectively. The Monkhorst–Pack k-mesh of 3×3×1 for Cu-Ag and Cu was adopted. The threshold for force was set to -0.1 eV·Å^{-1}, and the Van der Waals (vdW) correction was adopted by Grimme (DFT+D3)[15].

The Cu-Ag and Cu surface were modeled using six-layer slab within (5×5) surface unit cell. The top four layers and the adsorbates were fully relaxed, and the remaining layers were fixed. To avoid the periodic interactions of the system, a vacuum region of 15 Å between two repeated slabs was used in the direction perpendicular to the surface.

The free energy change (ΔG) of each electrochemical step was calculated based on the computational hydrogen electrode (CHE) model. The Gibbs free energies of intermediates were calculated by the equation $\Delta G = \Delta G_0 + \Delta G(\mathrm{pH})$. The ΔG_0 was calculated at 298.15 K by the VASPKIT package[16], which according to $\Delta G_0 = \Delta E_{DFT} + \Delta E_{ZPE} - T\Delta S$. The E_{DFT}, E_{ZPE}, and S indicates the electronic energy, zero-point energy and entropy, respectively. . The free energy of H^+ ions was corrected by the concentration dependence of the entropy: $\Delta G(\mathrm{pH}) = -kT\ln[H^+] = kT\ln10\times\mathrm{pH}$. The experiment pH was 6.8 in this study.

Reference

1 X. Zou, A. Li, C. Ma, Z. Gao, B. Zhou, L. Zhu and Z. Huang, Nitrogen-doped carbon confined Cu-Ag bimetals for efficient electroreduction of CO_2 to high-order products, *Chem. Eng. J.*, 2023, 468, 143606.

2 P. Iyengar, M. J. Kolb, J. R. Pankhurst, F. Calle-Vallejo and R. Buonsanti, Elucidating the Facet-Dependent Selectivity for CO_2 Electroreduction to Ethanol of Cu-Ag Tandem Catalysts, *ACS Catal.*, 2021, 11, 4456-4463.

3 D. Shu, M. Wang, F. Tian, H. Zhang and C. Peng, A dual-cathode study on Ag-Cu sequential CO_2 electroreduction towards hydrocarbons, *J CO_2 Util.*, 2021, 45, 101444.

4 C. Choi, J. Cai, C. Lee, H. M. Lee, M. Xu and Y. Huang, Intimate atomic Cu-Ag interfaces for high CO_2RR selectivity towards CH4 at low over potential, *Nano Res.*, 2021, 14, 3497-3501.

5 Z. Ma, T. Wan, D. Zhang, J. A. Yuwono, C. Tsounis, J. Jiang, Y. H. Chou, X. Lu, P. V. Kumar, Y. H. Ng, D. Chu, C. Y. Toe, Z. Han and R. Amal, Atomically Dispersed Cu Catalysts on Sulfide-Derived Defective Ag Nanowires for Electrochemical CO_2 Reduction, *ACS Nano*, 2023, 17, 2387-2398.

6 W. Su, W. Guo and Y. Fan, CuAg bimetallic catalysts derived from an Ag-anchored Cu-based metal-organic framework for CO_2 electroreduction to ethanol, *Chem. Eng. J.*, 2023, 477, 147204.

7 Z. Chang, S. Huo, W. Zhang, J. Fang and H. Wang, The Tunable and Highly Selective Reduction Products on Ag@Cu Bimetallic Catalysts Toward CO_2 Electrochemical Reduction Reaction, *J. Phys. Chem. C*, 2017, 121, 11368-11379.

8 W. Zhang, C. Xu, Y. Hu, S. Yang, L. Ma, L. Wang, P. Zhao, C. Wang, J. Ma and Z. Jin, Electronic and geometric structure engineering of bicontinuous porous Ag-Cu nanoarchitectures for realizing selectivity-tunable electrochemical CO_2 reduction, *Nano Energy*, 2020, 73, 104796.

9 T. Zhang, Y. Liu, C. Yang, L. Tian, Y. Yan and G. Wang, Monotonically increasing relationship between conversion selectivity from CO_2 to CO and the interface area of Cu-Ag biphasic electrochemical catalyst, *J. Alloy Compd.*, 2023, 947, 169638.

10 G. Kresse and J. Hafner, Ab initio molecular dynamics for liquid metals, *Phys. Rev. B*,, 1993, **47**, 558.

11 G. Kresse and J. Hafner, Ab initio molecular-dynamics simulation of the liquid-metal–amorphous-semiconductor transition in germanium, *Phys. Rev. B*, 1994, **49**, 14251.

12 G. Kresse and J. Furthmüller, Efficient iterative schemes for ab initio total-energy calculations using a plane-wave basis set, *Phys. Rev. B*, 1996, **54**, 11169.

13 J. P. Perdew, K. Burke and M. Ernzerhof, Generalized gradient approximation made simple, *Phys. Rev. Lett.*, 1996, **77**, 3865.

14 P. E. Blöchl, Projector augmented-wave method, *Phys. Rev. B*, 1994, **50**, 17953.

15 S. Grimme, Density functional theory with London dispersion corrections, *Wires. Comput. Mol. Sci.*, 2011, **1**, 211-228.

16 V. Wang, N. Xu, J.-C. Liu, G. Tang and W.-T. Geng, VASPKIT: A user-friendly interface facilitating high-throughput computing and analysis using VASP code, *Comput. Phys. Commun.*, 2021, **267**, 108033.